Pediatr Blood Cancer 2004;42:268–274

Biodistribution of Post-Therapeutic Versus Diagnostic ^{131}I-MIBG Scans in Children With Neuroblastoma†

Marc P. Hickeson, MD, Martin Charron, MD,* John M. Maris, MD, Patricia Brophy, CRNP, Tammy I. Kang, MD, Hongming Zhuang, MD, PhD, Jehanzeb Khan, MD, and Teresa Nevrotski, CNMT

Background. To evaluate the biodistribution of therapeutic ^{131}I-metaiodobenzylguanidine (MIBG) and assess the sensitivity of diagnostic versus therapeutic ^{131}I-MIBG scans to detect metastatic disease. ***Procedure.*** This retrospective study included 44 diagnostic and post-therapy scans (PTS) in 18 children with neuroblastoma treated with ^{131}I-MIBG (2.0–33.1 GBq). The findings of diagnostic scans (DS) (2.6–44.4 MBq) were compared to those of corresponding PTS. ***Results.*** In terms of biodistribution, the PTS identified ^{131}I-MIBG activity in one or more patients in the following regions not detected on the DS: nasal mucosa, cerebellum, central brain, adrenals, spleen, kidneys, thyroid, salivary glands, lower halves of the lungs, bladder, bowel, and an incisional scar. Conversely, the DS identified activity in the thorax, heart, kidneys, and bladder each in one patient without being visualized on the PTS. In terms of sensitivity to detect metastatic disease, 210 lesions were seen on the PTS compared to 151 on the DS. The PTS demonstrated sites of disease not evident in the DS in 16 cases. ***Conclusions.*** The biodistribution of ^{131}I-MIBG is different using therapeutic doses as compared to pre-therapy doses. ^{131}I-MIBG imaging following high therapeutic doses often reveals sites of occult metastatic disease that may be clinically relevant. Pediatr Blood Cancer 2004;42:268–274. © 2003 Wiley-Liss, Inc.

Key words: biodistribution; iodobenzylguanidine; metastases; neuroblastoma; neuroblastoma diagnosis; neuroblastoma therapy

INTRODUCTION

Neuroblastoma is the most commonly diagnosed extracranial solid pediatric malignancy in the first year of life [1]. It represents 7% of all pediatric cancers and is the cause of 15% of all childhood cancer deaths [2]. There are 8.7 new cases per million children or 500–600 new cases annually in the US [1]. Neuroblastoma arises from neural crest derived sympathetic nervous system precursor cells. It is a clinically heterogeneous disease with patient outcome tightly correlated with patient age at diagnosis, local and metastatic extent of disease, and tumor biologic features such as the presence or absence of the n-myc oncogene amplification. At diagnosis, metastatic disease is identified in half of infants and in two thirds of children aged 1 year and older [3]. The most common sites of metastases are cortical bone and bone marrow as well as both regional and distant lymph nodes. Infants often show disease dissemination to the liver and subcutaneous tissues.

The diagnostic modalities that are used for determining the disease extent include bone marrow aspirates and biopsies, CT scan, MRI, ^{99m}Tc-MDP bone scan, and ^{131}I-MIBG or ^{123}I-MIBG scan [2]. The sensitivity and specificity of MIBG are very high because most neuroblastomas take up MIBG [4].

The treatment of neuroblastoma depends on a risk category assignment that is based on the analysis of host of patient-specific and tumor-specific variables. However, over 50% of patients are categorized as high-risk due mainly to widespread disseminated disease in patients older than 1 year at diagnosis. These patients receive aggressive multimodal treatment including chemotherapy, radiation therapy, surgery, myeloablative chemotherapy followed by stem cell rescue, and biologic response modifiers [5]. Despite this, the long-term prognosis of advanced neuroblastoma remains poor with current survival probabilities of less than 30%.

Since ^{131}I-MIBG concentrates in neuroblastoma tumors, it is potentially capable of selectively delivering a substantial radiation dose to the neuroblastoma cells in both primary tumors and metastases [4]. ^{131}I-MIBG therapy has been used in children with neuroblastoma who were resistant to conventional therapy and, more recently, as front line therapy with promising results [4–13].

There is however some evidence that some metastases that may be too small or too defective in trapping MIBG

The Children's Hospital of Philadelphia, 34th and Civic Center Boulevard, Philadelphia, Pennsylvania

†This manuscript was originally submitted to and accepted for publication in *Medical & Pediatric Oncology* by it's Editor-in-Chief, Dr. G. D'Angio.

*Correspondence to: Martin Charron, Director, Division of Nuclear Medicine, Department of Radiology, The Children's Hospital of Philadelphia, 34th and Civic Center Boulevard, Philadelphia, PA 19104. E-mail: charron@email.chop.edu

Received 16 October 2002; Accepted 23 September 2003

DOI 10.1002/pbc.10454

to be visualized on the DS may be visualized when the patient returns for imaging a few days after the treatment dose of MIBG [14,15]. Recently, Fatourechi et al. reported abnormal ^{131}I uptake in 13% of patients with differentiated thyroid cancer on the PTS in areas that were not seen on the DS [16]. The purpose of this study is to compare the difference in the biodistribution and sensitivity in the detection of metastatic disease with the DS and the PTS using ^{131}I-MIBG in patients with neuroblastomas. The difference of the biodistribution of diagnostic and therapeutic ^{131}I-MIBG and the sensitivity for the detection of metastatic disease have not been analyzed simultaneously on any study.

MATERIALS AND METHODS

Patients

Twenty-four patients: 10 males and 14 females aged 1.5–22.0 years (mean 8.9 years) were treated with ^{131}I-MIBG over a period of 13 years. Twenty three patients had neuroblastoma and one had pheochromocytoma. Eighteen of these patients with neuroblastoma had ^{131}I-MIBG DS performed in our institution and these were compared with their corresponding ^{131}I-PTS. Out of these 18 patients, two had two pairs of DS and PTS and one had three pairs of DS and PTS. The total of pairs of DS and PTS was 22. Institutional Review Board approval was obtained for this retrospective study.

Imaging Protocols

For the DS, all patients were treated with SSKI on an adult dose of three drops daily beginning 1 day before the radiopharmaceutical injection and continuing for 6 days after tracer administration. The dose of ^{131}I-MIBG was 37 MBq/1.73 m^2 (range: 2.6–44.4 MBq, mean: 17.8 MBq). Imaging was performed with a high-energy collimator at 48 hr after injection at 15 min per image. All images contained 256×256 pixels.

For the PTS, all patients were treated with SSKI on an adult dose of three drops daily starting 1 day before and ending 6 weeks after radiopharmaceutical administration. They were also given an anti-emetic about 1 hr prior to the therapeutic dose. The dose administered (range: 2.0–33.1 GBq, mean: 7.8 GBq) was determined either by dosimetry using a tracer dose of ^{131}I-MIBG or by fixed dose of 444–666 MBq/kg depending on the phase of the trial. The therapeutic radiopharmaceutical was delivered from Ann Arbor, Michigan in the frozen state. After thawing, the prescribed dose was drawn up in a 60 ml syringe and diluted with normal saline to total volume of 30 ml. The shielded syringe was delivered to the patient's room. It was then placed in a Medfusion 2010 infusion pump, situated behind lead bricks, connected to the patient's venous access line, and administered over 90 min. At the end of the infusion, a suitable saline flush was used to clear the line of residual radiopharmaceutical. After this time, the radiation level was monitored by radiation safety until it was less than 0.07 mSv/hr at 1 m at which time the patient was discharged. Prior to discharge, a total body scan was obtained with a high energy collimator at 2 min per image and 256 × 256 pixels per image.

The same fields of view were compared between the DS and PTS. A lesion independent of its size is considered as one diseased site (i.e., one large lesion and one small focus each count as one diseased site). If the PTS detected an extension of the activity demonstrated on the DS, this would not be considered as additional diseased site unless that the new site is not contiguous to that detected in the DS. Conversely, if the DS scan detected two lesions that appeared as one larger lesion on the PTS, then this lesion would have been considered as one diseased site on both the DS and the PTS. All studies were reviewed by two nuclear medicine physicians in consensus.

RESULTS

In terms of the biodistribution (Table I), the PTS demonstrated MIBG activity in the following regions not detected on the DS: nasal mucosa (N = 11), cerebellum (N = 5) (Fig. 1), central brain region (N = 5), adrenals (N = 3), spleen (N = 3), kidneys (N = 3), thyroid (N = 2), salivary glands (N = 1), lower halves of the lungs (N = 1), urinary bladder (N = 1), bowel (N = 1), and an incisional scar (N = 1). Conversely, the DS identified activity in the following regions not detected on the PTS: thorax (N = 1), heart (N = 1), kidneys (N = 1), and urinary bladder (N = 1). The uptake at all of these sites was considered as normal physiological distribution on the basis of the symmetry of uptake, similar site, and shape in different patients, and absence of any clinical manifestation of malignancy at these sites on follow up.

In terms of the sensitivity for detecting neoplastic disease, abnormal uptake was detected in all 22 of 22 PTS (100%) and compared to 21 of 22 DS (95%). The PTS demonstrated sites of disease that were not evident in the DS in 16 of 22 cases (73%) and increased the confidence in detecting an additional lesion in another patient (5%). Two hundred ten lesions were detected on the PTS as compared to 151 on the DS, which represents 59 out of 151 (39%) more lesions seen on the PTS. An example is shown in Figure 2. The PTS upstaged the disease in 1 case of 22 (5%) and increased the confidence in diagnosing stage 4 disease in another patient. In one case, no disease was demonstrated on the DS in a patient considered to be in complete remission, and the PTS scan showed abnormal uptake in the left humerus (Fig. 3). In the other case, a subtle lesion was seen in the liver on the DS that was definite on the PTS.

TABLE I. Biodistribution of the Diagnostic and Therapeutic ^{131}I-MIBG Images

Patient number	Age/sex	Sites imaged	Diagnostic scan biodistribution	Therapeutic scan biodistribution
1	6y 11m F	Whole body	Injection site (R upper chest), salivary glands, nose, heart, liver, bladder	Injection site (R upper chest), salivary glands, nasal mucosa, heart, spleen, liver, bladder, kidneys
2a	9y 10m F	Whole body	Salivary glands, nasal mucosa, heart, liver, bladder, soft tissues	Salivary glands, nasal mucosa, central brain, liver, heart, bladder, urethra, both adrenals
2b	10y F	Whole body	Salivary glands, nasal mucosa, heart, liver, spleen, kidneys, bladder, soft tissues	Salivary glands, nasal mucosa, central brain, thyroid, liver, spleen, kidneys, bladder
3a	10y 5m M	Abdomen and pelvis	Kidneys	Kidneys
3b	10y 10m M	Whole body	Salivary glands, liver, kidneys, heart	Salivary glands, nasal mucosa, cerebellum, central brain, kidneys, liver
4	8y 7m F	Whole body	Liver, spleen, salivary glands, heart, lungs, kidneys	Liver, spleen, salivary glands, heart, lungs, kidneys, nasal mucosa, cerebellum
5	22y F	Abdomen only	Liver, bladder	Liver, kidneys, bladder, soft tissues, abdominal scar, both adrenals
6	4y 10m M	Whole body	Salivary glands, heart, liver, bladder	Salivary glands, central brain, cerebellum, nasal mucosa, heart, liver, spleen, bladder
7	5y 4m F	Abdomen only	No significant uptake in normal tissue	Bladder
8	2y F	Whole body	Salivary glands, heart, liver, bladder, nose	Salivary glands, heart, liver, bladder, nasal mucosa, lower 1/2 of lungs, cerebellum
9	12y 4m F	Whole body	Salivary glands, thyroid, liver, bladder	Salivary glands, nasal mucosa, central brain, thyroid, liver, bladder
10	2y 1m F	Lower head to hips	Salivary glands, heart, liver, kidneys, bladder	Salivary glands, nasal mucosa
11a	12y 4m M	Whole body	Salivary glands, liver	Salivary glands, liver, nasal mucosa
11b	12y 6m M	Whole body	Salivary glands, thorax, liver, bladder	Salivary glands, liver, nasal mucosa
11c	12y 10m M	Whole body	Salivary glands, liver, bladder	Salivary glands, liver, nasal mucosa, bladder
12	1y 2m F	Whole body	Salivary glands, heart, liver, bladder	Salivary glands, nasal mucosa, cerebellum, heart, liver, bladder
13	15 y7m F	Lower head to lower limbs	Salivary glands, nasal mucosa, heart liver, bladder	Salivary glands, liver, bladder
14	1y 6m F	Whole body	Heart, liver	Heart, liver, bladder
15	4y 4m F	Thorax, abdomen, pelvis	Liver	Liver, heart
16	7y 4m M	Posterior abdomen, thorax, and proximal upper limbs	Heart, liver, bladder	Heart, liver, bladder, kidneys, adrenals, spleen, bowel
17	3y 9m M	Whole body	Salivary glands, nasal mucosa, liver, bladder	Salivary glands, nasal mucosa, liver
18	9y 4m M	Whole body down to mid femora	Liver, bladder	Salivary glands, nasal mucosa, thyroid, liver, bladder

y, year; m, month.

When correlating to the dose per weight for the DS, the PTS revealed greater disease burden (Table II) in all three of three patients (100%) as compared to DS with doses of less than 0.5 MBq/kg and upstage the disease in none of the patients. The PTS detected more sites of disease in 9 of 12 patients (75%) as compared to DS with a dose between 0.50 and 0.99 MBq/kg and upstaged in one case (9%). The PTS resulted in increased number of disease sites in four of seven patients (57%) than on the DS scans with doses of 1.0 MBq/kg or higher and increased the confidence in detecting an additional lesion and upstage to stage 4 disease in one of seven patients (14%). When correlating to the dose per weight for the PTS, greater disease burden was demonstrated in 4 of 5 patients (80%), 4 of 7 patients (57%), and 8 of 10 patients (80%) for doses of less than 200 MBq/kg, 200–349 MBq/kg, and 350 MBq/kg or higher, respectively, as compared to the DS. The PTS upstaged the disease in 1 of 10 patients (10%) with a dose of 350 MBq/kg and increased the confidence of diagnosing stage 4 disease in 1 of 7 patients (57%) with a dose between 200 and 249 MBq/kg.

DISCUSSION

^{131}I-MIBG is radioiodinated analogue of norepinephrine [17]. The chemical structure includes the benzyl

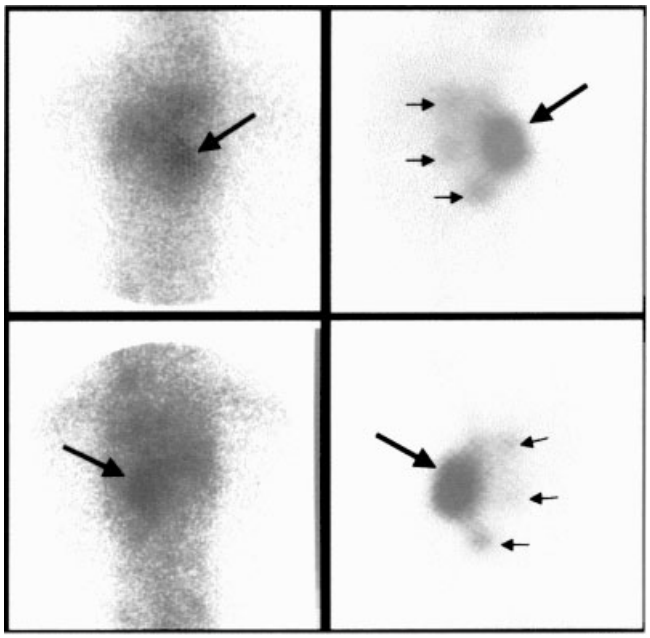

Fig. 1. The post-therapy scan shown in the **anterior** (**bottom left**) and **left lateral** (**bottom right**) projections demonstrates subtle physiologic MIBG activity in the central brain (arrow) and posterior fossa (arrow) in this 4 year-old-boy (patient #6) with a history of neuroblastoma, which was not seen on the diagnostic scan shown in the anterior (**top left**) and **right lateral** (**top right**) projections.

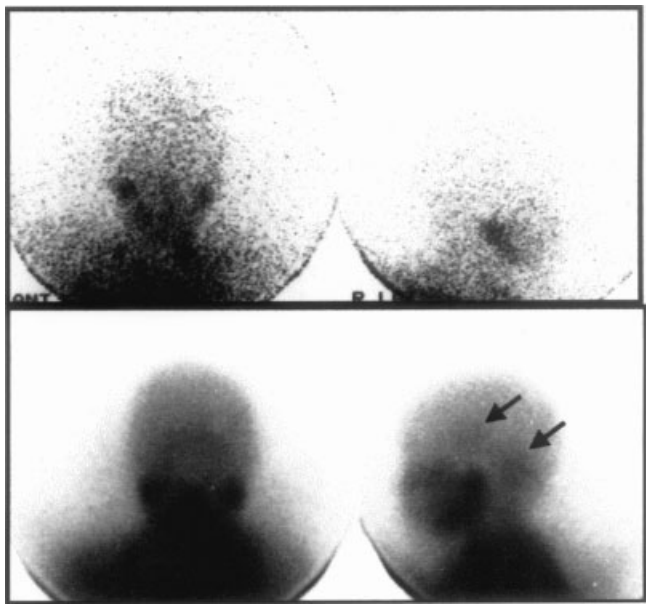

Fig. 3. This 7-year-old boy (patient #16) with a history of neuroblastoma was apparently disease-free on the diagnostic scan (**left**). The post-therapy scan (**right**) demonstrates a small lesion in the left proximal humerus. Both scans are shown in the posterior projection.

portion of bretylium with the guanidine group of guanethidine. The cellular uptake of MIBG into adrenomedullary cells is similar to norepinephrine. It takes place by two mechanisms: uptake-1 and uptake-2 [2,12,18]. Uptake-1 is an active process by the noradrenaline transport transmembrane protein and is a high affinity, saturable, sodium, energy, and temperature-dependent process. In contrast, uptake-2 is a non-specific mechanism, presumed to be passive diffusion and energy independent and unsaturable at concentrations of at least 5 mM.

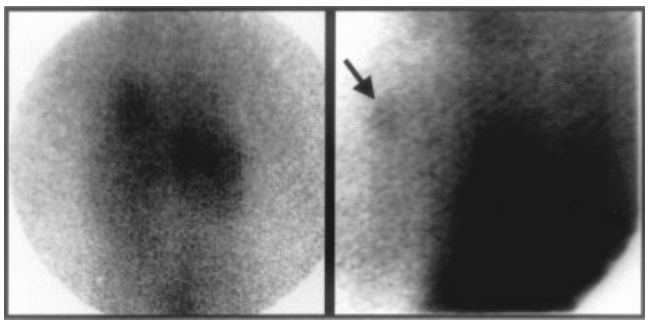

Fig. 2. This one and a half-year-old girl (patient #14) has a large left adrenal mass (large arrows) seen on the diagnostic (**left**) and post-therapeutic images (**right**) obtained in the **anterior** (**top**) and **posterior** (**bottom**) projections. The post-therapeutic images demonstrate intense uptake in the large left abdominal mass and an additional three intra-abdominal lesions (small arrows) not seen on the diagnostic images.

In this study, MIBG uptake was observed in several sites on the PTS not evident on the DS. As the plasma concentrations of MIBG is <0.1 μM in therapeutic doses of carrier-free ^{131}I-MIBG, uptake-1 is the predominant mechanism of uptake [18]. However, uptake-2 becomes increasingly less negligible in terms of the contribution of MIBG uptake at higher doses in the PTS. The spleen, the nasal mucosa, and the adrenals are all very vascular structures. The MIBG activity in the central brain probably represents the locus ceruleus in the brain stem and this structure and the cerebellum both contain relatively high density of adrenergic neurons [19]. Other observers have also demonstrated MIBG activity in the lung on the PTS that was not seen on the DS [20]. Possible explanations for the uptake in structures only seen using high doses of MIBG are by three possible mechanisms: by higher count densities provided by PTS, depending on the perfusion, and by the second mechanism of MIBG uptake.

Treatment with ^{131}I-MIBG has been used in children with neuroblastoma for palliative and, recently, curative purposes. According to the cumulative experience of several centers, the overall objective response rate is approximately 35% in patients with chemoresistant neuroblastoma after induction chemotherapy or at relapse [13]. There are currently four major methods for determining the therapeutic dose to be delivered: by dosimetry using a tracer dose of MIBG, by dose per body weight, by fixed dose, and by dose escalation in which hematopoietic tissue is harvested for bone marrow transplant [4]. In our institution, ^{131}I-MIBG therapy is given to patients

TABLE II. Disease Burden Determined by the Diagnostic and Post-Therapeutic ^{131}I-MIBG Scans

Patient number	Weight (kg)	Dose on DS (MBq)	Dose/Wt on DS (MBq/kg)	Dose on PTS (GBq)	Dose/Wt on PTS (MBq/kg)	Delay of PTS (days)	Disease sites on DS	New sites on PTS	Stage on DS	Stage on PTS	Number of sites on DS	Number of sites on PTS
1	11.7	11.1	0.96	4.29	366.3	43	Mediastinum, skull, pelvis, femora	L supraclavicular region, tibiae	IV	IV	4	7
2a	18.1	17.5	0.96	6.55	362.6	10	L humerus, L thorax, R iliac, L femur	No new sites	IV	IV	4	4
2b	18.2	18.9	1.04	6.73	370.0	3	L humerus, L thorax	L femur, R iliac	IV	IV	2	4
3a	20.4	17.0	0.85	3.63	177.6	3	Large abdominal mass	Abdominal cavity	III	III	5	6
3b	20.3	22.2	1.07	4.37	214.6	29	Large abdominal mass	Abdominal cavity	III	III	5	8
4	14.6	14.6	1.00	2.59	177.6	31	Large abdominal mass	No new sites	III	III	1	1
5	47.6	44.4	0.93	13.91	292.3	16	Right abdominal mass	No new sites	IIA	IIA	1	1
6	17.6	15.5	0.89	5.85	333.0	34	R paraspinal and L cervical regions	Abdominal cavity	IV	IV	2	5
7	7.0	11.1	1.59	3.66	521.7	28	Large abdominal mass	No new sites	III	III	1	1
8	10.0	12.7	1.26	4.22	421.8	8	R adrenal, R thorax	L lung	IV	IV	2	3
9	34.7	29.6	0.85	7.59	218.3	8	Skull, ribs, L humerus, spine, pelvis, femora	Skull, ribs, spine, humeri	IV	IV	35	51
10	12.7	14.1	1.11	6.59	518.0	8	Thorax, abdomen	Mediastinum, pelvis, abdomen	IV	IV	3	7
11a	26.5	20.4	0.78	9.51	358.9	8	Skull, axial skeleton, appendicular skeleton	Humeri, R ulna	IV	IV	14	17
11b	25.6	21.8	0.85	9.29	362.6	5	Skull, axial skeleton, appendicular skeleton	Tibiae, radii, ulnae, carpal regions, ribs	IV	IV	14	26
11c	26.0	25.5	1.00	9.62	370.0	15	Skull, axial skeleton, appendicular skeleton	Skull	IV	IV	26	27
12	15.5	14.1	0.93	5.33	344.1	17	Large abdominal mass	No new sites	III	III	1	1
13	34.7	37.0	1.07	9.25	266.4	26	Abdominal cavity, questionable liver	More defined liver lesion	III or IV	IV	6 or 7	7
14	9.7	2.6	0.26	2.52	259.0	51	Abdomen, pelvis, L supraclavicular region	Abdomen, pelvis, appendicular skeleton	IV	IV	6	8
15	14.5	13.0	0.89	2.04	140.6	15	Abdomen, spine, pelvis, R femur	L humerus	IV	IV	4	
16	13.7	11.5	0.85	5.74	418.1	8	No active disease	L humerus	I	IV	0	1
17	46.9	14.8	0.33	8.51	181.3	22	Femora, tibiae	Mid T spine	IV	IV	11	12
18	34.6	15.2	0.44	6.66	192.4	15	Mediastinum, upper abdomen, ant. skull	Skull, pelvis, R femur	IV	IV	3	7

who are categorized as high risk and are refractory to chemotherapy.

The PTS increased the estimated disease burden in 16 cases (73%) and detected 39% more lesions than the corresponding DS. The PTS upstaged one case and increased the confidence in diagnosing stage 4 disease in another in which a questionable lesion in the liver seen on the DS and was definite on the PTS. In the other case, the DS scan demonstrated an apparently complete response to chemotherapy with no active lesions seen; however, a lesion in the left humerus was seen on the PTS. Since the PTS detects more diseased sites than the DS, assessing treatment response from a therapeutic dose of ^{131}I-MIBG with the DS is difficult. The increase of number of lesions seen on the PTS is thought to be due to the high activity of ^{131}I-MIBG providing higher count densities and, consequently, higher lesion's signal to background ratios than seen on the DS. Parisi et al. attributed the detectability of lesions as a function of contrast and spatial frequency composition [15]. This study also reported a greater sensitivity of the ^{131}I-MIBG PTS as compared to the DS in 14 patients [15]. Similar conclusions were observed with ^{131}I scanning using diagnostic and therapeutic doses for differentiated thyroid cancer for similar reasons [21–23]. It would also be interesting to compare the sensitivity of detection of metastatic lesions with ^{123}I-MIBG scintigraphy and with the ^{131}I-MIBG PTS. The diagnostic scans (DS) with ^{123}I-MIBG probably provide higher sensitivity for disease detection and lower radiation doses to patients than with those using ^{131}I-MIBG. However, a correlation to the dose with the sensitivity cannot be determined on this study when analyzing the DS or the PTS individually.

The limitations of this study are the lack of tissue biopsy for confirmation and the lack of perfect method in quantifying the number of diseased sites. MIBG uptake has been previously described in the salivary glands, thyroid (likely due to free iodine), heart, spleen, bowel, kidney, and bladder [24]. Fortunately, the other MIBG-avid tumors [25–34] are relatively uncommon in children, which explain the high positive predictive value of focal MIBG uptake for neuroblastoma in children. In addition, the sites of physiologic uptake were confirmed with the absence of any manifestation of malignancy on clinical follow up. The gold standard considered on this study was the number of individual sites demonstrated on the PTS. The method we adopted to determine the disease burden was to count the number of diseased sites observed on the DS scan and the PTS. Because the size of the lesions was not considered for disease involvement, this is not a perfectly accurate method to determine the disease burden. It is, however, a relatively reproducible method to compare the disease extent between the DS and the PTS.

MIBG scintigraphy remains the most sensitive modality for the detection of neuroblastoma. However, a small percentage of neuroblastoma lesions demonstrate a lack of avidity to MIBG. Biasotti et al. reported a 8% false negative rate in all patients with neuroblastoma [35]. If children with stages 1 or 2 disease only are considered, the false-positive rate was as high as 24%. This lack of avidity can be indicative of highly anaplastic neuroblastomas or in more mature neoplasms such as ganglioneuromas [36]. If lesions not avid to MIBG are present, then therapy with ^{131}I-MIBG will not be helpful and the patient will be spared from having futile therapy.

CONCLUSIONS

All patients were treated as inpatient with ^{131}I-MIBG. For this reason, they are readily accessible to return for imaging. Scanning after therapy does not pose any additional radiation risks. The PTS increases the confidence of detecting lesions seen on the DS as well as the number of lesions detected and may upstage the disease in a small number of patients. The biodistribution of MIBG is different using therapeutic doses as compared to the diagnostic doses and the PTS greatly improved the precision for detecting extent of disseminated disease.

ACKNOWLEDGMENT

The authors are indebted to the significant contribution by Dr. Sydney Heyman, MD and all of the nuclear medicine technologists for having prepared an archiving system with all of the patients treated with I-131 MIBG. The authors are also thankful for the excellent administrative work of Melissa Bennett and Angela Dorman from the Department of Radiology.

REFERENCES

1. Young JL, Riesl LG, Silverberg E, et al. Cancer incidence, survival, and mortality for children under 15 years of age. Cancer 1986; 58:598–602.
2. Shulkin BL, Shapiro B. Current concepts on diagnostic use of MIBG in children. J Nucl Med 1998;39:679–688.
3. Pizzo PA, Poplack DG, Morowitx ME, et al. Solid tumors of childhood. In: Devita VT, Hellman S, Rosenberg SA, editors. Cancer: Principles and practice of oncology. 4th edn. Philadelphia, PA: Lippincott; 1993. pp 1738–1791.
4. Tepmongkol S, Heyman S. ^{131}I MIBG therapy in neuroblastoma: Mechanisms, rationale, and current status. Med Pediatr Oncol 1999; 32:427–431.
5. Klingebiel T, Bader P, Bares R, et al. Treatment of neuroblastoma stage 4 with ^{131}I-meta-iodo-benzylguanetidine, high dose chemotherapy, and immunotherapy. A pilot study. Eur J Cancer 1998; 34:1398–1402.
6. Hartman O, Lumbroso J, Lemerle J, et al. Therapeutic use of ^{131}I-MIBG in neuroblastoma: A phase II study in nine patients. Med Pediatr Oncol 1987;15:205–211.
7. Hoefnagel CA, deKraker J, Voute PA, et al. Preoperative ^{131}I-MIBG therapy of neuroblastoma at diagnosis (''MIBG de novo''). J Nucl Biol Med 1991;35:248–251.
8. Treuner J, Gerein V, Klingebiele T, et al. MIBG treatment in neuroblastoma; experiences of the Tuebingen/Frankfort group. Prog Clin Biol Res 1988;271:669–678.

9. Mastranglo R, Tornesello A, Mastrangelo S. Role of ^{131}I-metaiodobenzylguanedine in the treatment of neuroblastoma. Med Pediatr Oncol 1998;31:22–26.
10. Goldberg SS, Desantes K, Huberty JP, et al. Engraftment after myeloablative doses of 131-metaiodobenzylguanidine followed by autologous bone marrow transplantation for treatment of refractory neuroblastoma. Med Pediatr Oncol 1998;30:339–346.
11. Gaze MN, Wheldon TE, O'Donoghue JA, et al. Multimodality megatherapy with [^{131}I] metaiodobenzylguanidine, high dose melphalan, and total body irradiation with bone marrow rescue: Feasibility study of a new strategy for advanced neuroblastoma. Eur J Cancer 1995;31:252–256.
12. Meller S. Targeted radiotherapy for neuroblastoma. Arch Dis Child 1997;77:389–391.
13. Troncone L, Galli G. Proceedings of international workshop on the role of ^{131}I metaiodobenzylguanidine in the treatment of neural crest tumors. J Nucl Biol Med 1991;35:177–362.
14. Giammante F, Lumbroso J, Richard N, et al. Radioiodinated metaiodobenzylgauanidine in neuroblastoma: Influence of high dose on tumour site detection. Eur J Nucl Med 1995;22:1180–1183.
15. Parisi MT, Matthay KK, Huberty JP, et al. Neuroblastoma dose-related sensitivity of MIBG scanning. Radiology 1992;184:463–467.
16. Fatourechi V, Hay ID, Mullan BP, et al. Are posttherapy radioiodine scans informative and do they influence subsequent therapy of patients with differentiated thyroid cancer? Thyroid 2000;10:573–577.
17. Sisson JC, Wieland DM, Sherman P, et al. Metaiodobenzylguanidine as an index of the adrenergic nervous system integrity and function. J Nucl Med 1987;28:1620–1624.
18. Iavarone A, Lasorella A, Servidir T, et al. Uptake and storage of MIBG are frequent neural functions of human neuroblastoma cell lines. Cancer Res 1993;53:304–309.
19. Harttner RS, Pounds TR, Matthay KR. Normal cerebellar MIBG localization implications in the interpretation of delayed scans. Clin Nucl Med 1994;19:985–988.
20. Bonnin F, Lumbroso J, Tenenbaum F, et al. Refining interpretation of MIBG scan in children. J Nucl Med 1994;35:803–810.
21. Preisman R, Halpein S. Detection of metastatic thyroid carcinoma after the administration of a therapeutic dose of 131-iodine. Eur J Nucl Med 1978;3:69–70.
22. Pacini F, Lippi F, Fomina N, et al. Therapeutic doses of iodine-131 reveal undiagnosed metastases in thyroid cancer patients with detectable serum thyroglobulin levels. J Nucl Med 1987;28:1888–1891.
23. Bonnin F, Lumbroso J, Tenenbaum F, et al. Detection and treatment of lung metastases in patients with normal chest X-rays. J Nucl Med 1988;29:1790–1794.
24. Nakajo M, Shapiro B, Copp J, et al. The normal and abnormal distribution of the adrenomedullary imaging agent ^{131}I-iodobenzylguanidine (^{131}I-MIBG) in man: Evaluation by scintigraphy. J Nucl Med 1983;24:672–682.
25. Feldman JM, Blinder PA, Lucas KJ, et al. I-131 metaiodobenzylguanidine scintigraphy of carcinoid tumors. J Nucl Med 1986;27:1691–1696.
26. Von Moll L, McEwan AJ, Shapiro B, et al. MIBG scintigraphy of neuroendocrine tumors other than pheochromocytoma and neuroblastoma. J Nucl Med 1987;28:979–988.
27. Geatti O, Shapiro B, Barillari B. Scintigraphic depicting on an insulinoma by I-131 metaiodobenzylguanidine. Clin Nucl Med 1989;14:903–905.
28. Kaltsas G, Korbonits M, Heintz E, et al. Comparison of somatostatin analog and meta-iodobenzylguanidine radionuclides in the diagnosis and the localization of advanced neuroendocrine tumors. J Clin Endocrinol Metab 2001;86:895–902.
29. Castagnoli A, Biti G, DeCristofaro MT, et al. Merkel cell carcinoma and iodine-131 metaiodobenzylguanidine scan. Eur J Nucl Med 1992;19:913–916.
30. Rainis T, Ben-Haum S, Dickstein G. False-positive metaiodobenzylguanidine in a patient with a huge adrecortical carcinoma. J Clin Endocrinol Metab 2000;85:5–7.
31. Letizia C, Detoma G, Massa R, et al. False-positive diagnosis of adrenal pheochromocytoma on iodine-123 MIBG scan. J Clin Endocrinol Metab 1998;21:779–783.
32. Osei-Bonsu A, Kokoschka EM, Ulrich W, et al. ^{131}I-metaiodobenzylguanidine (mIBG) for bronchial oat cell cancer and melanoma detection. Eur J Nucl Med 1989;15:629–631.
33. Wadler S, Tai K, Cherviu LR, et al. Iodine-131 MIBG scintigraphy in small cell lung cancer. Eur J Nucl Med 1989;15:108–110.
34. Hayward RS, Bowering CK, Warshawski RS. I-131 metaiodobenzylguanidine uptake in a parathyroid adenoma. Clin Nucl Med 1988;13:632–634.
35. Biasotti S, Garaventa A, Villavecchia GP, et al. False-negative metaiodobenzylguanidine scintigraphy at diagnosis of neuroblastoma. Med Pediatr Oncol 2000;25:153–155.
36. Heyman S, Evan AE, D'Angio GJ. I-131 metaiodobenzylguanidine: Diagnostic use in neuroblastoma patients in relapse. Med Pediatr Oncol 1988;16:337–340.